SCIENTIFIC REP🜨RTS

OPEN

Aberrant Splicing Promotes Proteasomal Degradation of L-type Ca$_V$1.2 Calcium Channels by Competitive Binding for Ca$_V\beta$ Subunits in Cardiac Hypertrophy

Zhenyu Hu[1,*], Jiong-Wei Wang[2,3,*], Dejie Yu[1], Jia Lin Soon[4], Dominique P. V. de Kleijn[2,3,5], Roger Foo[3], Ping Liao[6], Henry M. Colecraft[7] & Tuck Wah Soong[1,8,9]

Decreased expression and activity of Ca$_V$1.2 calcium channels has been reported in pressure overload-induced cardiac hypertrophy and heart failure. However, the underlying mechanisms remain unknown. Here we identified in rodents a splice variant of Ca$_V$1.2 channel, named Ca$_V$1.2$_{e21+22}$, that contained the pair of mutually exclusive exons 21 and 22. This variant was highly expressed in neonatal hearts. The abundance of this variant was gradually increased by 12.5-folds within 14 days of transverse aortic banding that induced cardiac hypertrophy in adult mouse hearts and was also elevated in left ventricles from patients with dilated cardiomyopathy. Although this variant did not conduct Ca^{2+} ions, it reduced the cell-surface expression of wild-type Ca$_V$1.2 channels and consequently decreased the whole-cell Ca^{2+} influx via the Ca$_V$1.2 channels. In addition, the Ca$_V$1.2$_{e21+22}$ variant interacted with Ca$_V\beta$ subunits significantly more than wild-type Ca$_V$1.2 channels, and competition of Ca$_V\beta$ subunits by Ca$_V$1.2$_{e21+22}$ consequently enhanced ubiquitination and subsequent proteasomal degradation of the wild-type Ca$_V$1.2 channels. Our findings show that the resurgence of a specific neonatal splice variant of Ca$_V$1.2 channels in adult heart under stress may contribute to heart failure.

Cardiac excitation-contraction coupling is mainly initiated by Ca^{2+} influx through L-type voltage gated Ca$_V$1.2 channels in cardiomyocytes via Ca^{2+}-induced Ca^{2+} release mechanisms[1]. The Ca$_V$1.2 channel comprises a pore-forming α_1 subunit and auxiliary $\alpha_2\delta$ and β subunits[2]. The accessory subunits modulate the channel biophysical properties and are involved in the anchorage, trafficking and post-translational modification of the pore-forming α_1 subunit[3]. In particular, the Ca$_V\beta$ subunit was recently reported to promote the trafficking of Ca$_V$1.2 channels to the plasma membrane by inhibiting the proteasomal degradation of the channels[4]. Genetic deletion of either the pore-forming α_1 subunit or Ca$_V\beta$ subunit led to embryonic death with cardiac defects[5,6].

In cardiac hypertrophy and heart failure, linkage to alteration in Ca^{2+} influx via Cav1.2 channels has been controversial[7,8]. Clinical trials using Ca^{2+} channel blockers for heart failure have been disappointing with either no beneficial effects or a worse outcome of reduced ejection fraction[9–11]. Nevertheless, in human failing cardiomyocytes the density of Ca$_V$1.2 channels was decreased compared to normal cardiomyocytes[12]. In line with these findings, decreased Ca$_V$1.2 channel activity was recently reported to induce cardiac hypertrophy and heart failure

[1]Department of Physiology, Yong Loo Lin School of Medicine, National University of Singapore 117597, Singapore. [2]Department of Surgery, Yong Loo Lin School of Medicine, National University of Singapore, 117597, Singapore. [3]Cardiovascular Research Institute, National University Health Systems, Centre for Translational Medicine, 117599, Singapore. [4]National Heart Centre Singapore, 5 hospital drive, 169609, Singapore. [5]Dept of Cardiology, University Medical Center Utrecht, 3584CX Utrecht, The Netherlands. [6]Calcium Signaling Laboratory, National Neuroscience Institute, 11 Jalan Tan Tock Seng 308433, Singapore. [7]Department of Physiology and Cellular Biophysics, Columbia University, College of Physicians and Surgeons, New York, NY 10032, USA. [8]NUS Graduate School for Integrative Sciences and Engineering, 117456, Singapore. [9]Neurobiology/Ageing Programme, National University of Singapore, 117456, Singapore. *These authors contributed equally to this work. Correspondence and requests for materials should be addressed to T.W.S. (email: tuck_wah_soong@nuhs.edu.sg)
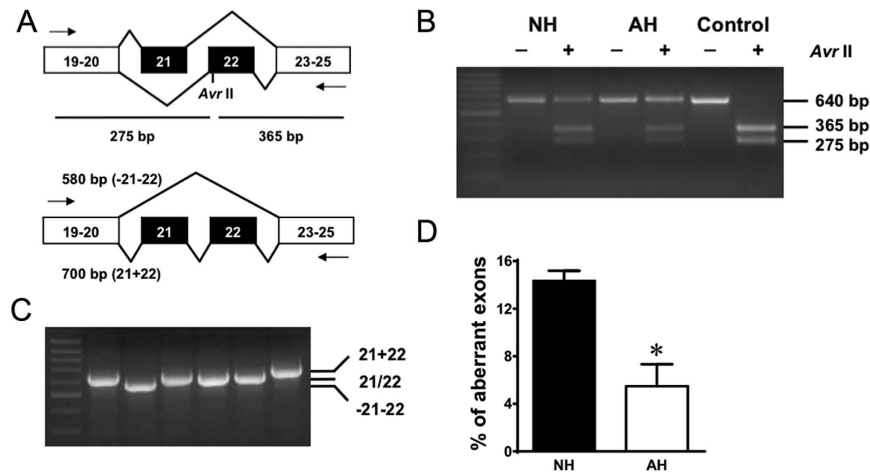
Figure 1. Inclusion level of exons 21+22 in $Ca_V1.2$ channels in neonatal hearts is higher than that in adult hearts. (**A**) Exons 21 and 22 are mutually exclusive exons. RT-PCR across exons 19–25 could generate a fragment of 640 bp. Digestion with AvrII could produce two smaller fragments of 275 bp and 365 bp. Besides, aberrant exclusion or inclusion of both exons 21 and 22 would generate two fragments of 580 bp and 700 bp, respectively. (**B**) mRNA of $Ca_V1.2$ channels from both neonatal (NH) and adult (AH) hearts showed partial digestion by AvrII. Complete digestion was observed in control DNA containing exon 22. (**C**) Colony screening of a neonatal heart identified bands of three size classes: 580 bp, 640 bp and 700 bp. (**D**) Summary of aberrant splicing rate in rat neonatal hearts (NH, n = 5) and adult hearts (AH, n = 5). Data were shown as mean ± SEM. *$p < 0.05$.

in genetically modified mice[8]. More importantly, the hypertrophied cardiomyocytes induced by pressure overload showed drastic decrease in $Ca_V1.2$ channel density and activity due to reduced expression of the $Ca_V1.2$ channels. The mechanisms, however, by which the density and activity of $Ca_V1.2$ channels were reduced is unknown.

The pore-forming α_1 subunit undergoes extensive alternative splicing that potentially generates multiple functionally diversified $Ca_V1.2$ variants in human[13] and rodent hearts[14]. Alternative splicing could be developmentally regulated[14,15] and involved in myocardial infarction[16] and heart failure[17]. In human diseases, alternative splicing of α_1 subunit has been reported in failing human ventricular cardiomyocytes and atherosclerotic human arteries[17,18]. Ectopic expression of some alternative splicing variants modulated the expression and activity of the $Ca_V1.2$ channels[5,14]. In the present study, we identified a $Ca_V1.2$ splice variant containing the mutually exclusive exons 21 and 22 (e21 + 22), named $Ca_V1.2_{e21+22}$ channel, which was highly expressed in neonatal and hypertrophied adult hearts. As the newly identified channel variant does not conduct Ca^{2+} ions, we hypothesized that it may account for the reduced expression and activity of $Ca_V1.2$ channels in hypertrophied cardiomyocytes induced by pressure overload[14].

Results

Differential expression of alternatively spliced isoforms of $Ca_V1.2$ channels in neonatal versus adult rat hearts.

Mutually exclusive exons 21 and 22 encode the IIIS2 transmembrane segment and part of the linker region between IIIS1 and IIIS2. Restriction enzyme AvrII digests within exon 22 only, but not exon 21 (Fig. 1A). RT-PCR across exons 19 to 25 produced a fragment of 640 bp in length. Control cDNA containing exon 22 only was completely digested by Avr II. Under similar conditions, however, only a portion of the RT-PCR products from both neonatal and adult hearts were digested, suggesting the presence of a mixture of PCR products expressing exon 21 and exon 22 in four possible combinations of e21, e22, e(21 + 22) and Δe(21 + 22) (Fig. 1B). The predicted PCR product sizes are 640 bp for e21 or e22, 700 bp for e(21 + 22) and 580 bp for Δe(21 + 22) (Fig. 1C). The results were confirmed by sequencing the PCR products. Inclusion of both exons will generate a channel with one additional transmembrane segment and may result in a drastic change in the topology of the channel. In this study, we focused on the splice variant including both exons e(21 + 22): $Ca_V1.2_{e21+22}$ channels. Transcript-scanning demonstrated that the abundance of $Ca_V1.2_{e21+22}$ channels in rat neonatal heart (14.3%) was 2.5 times higher than that in adult heart (5.5%, $P = 0.0124$, Fig. 1D).

Increased abundance of $Ca_V1.2_{e21+22}$ channels in hypertrophied heart.

Alteration in the expression of developmentally regulated $Ca_V1.2$ splice variants has been implicated in cardiac hypertrophy[19] and heart failure[17]. To examine whether the alternative splicing isoform $Ca_V1.2_{e21+22}$ in neonatal heart reemerges in the hypertrophic adult heart, we performed transverse aortic constriction (TAC) surgery on the mice as done previously[8] to generate pressure-overload induced cardiac hypertrophy that gradually develops and reaches a peak on day 14 after TAC surgery[20]. As expected, left ventricular (LV) weight to body weight, measured in isolated ventricles, increased significantly after two weeks of TAC (Fig. 2A). Thickening of left ventricular anterior and posterior walls at end diastole (d) or end systole (s) was overt via echocardiography (Fig. 2B,C and Table 1). Cardiac hypertrophy was also evidenced by the gradual increase in Myh7 and decrease in Myh6 at mRNA level
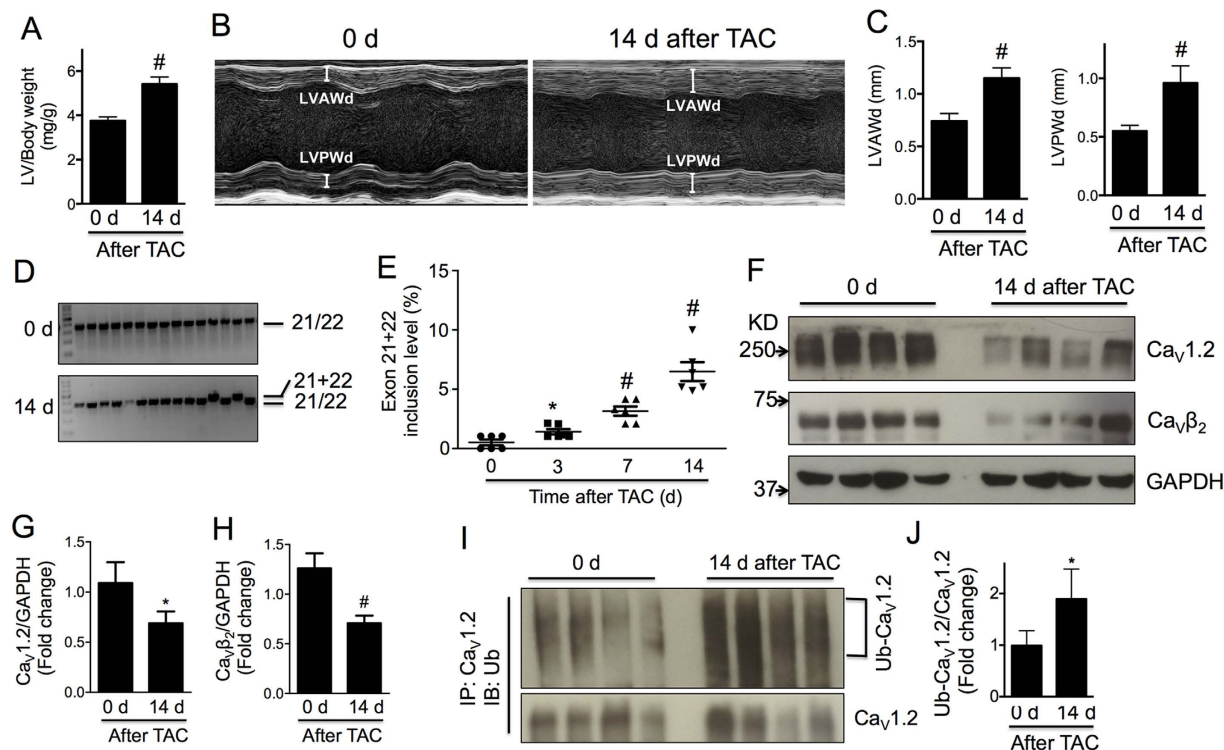
Figure 2. Abundance of cardiac $Ca_V1.2_{e21+22}$ channels is increased in mice in response to TAC surgery. (**A**) Increased ratio of left ventricle to body weight in TAC mice. (**B**) Representative M-mode echocardiography images of mouse hearts before and 14 days after TAC surgery indicating progression of cardiac hypertrophy. (**C**) Increased LVAWd and LVPWd in TAC mice. (**D**) Representative gel photos for transcript screening of exons $21 + 22$ inclusion level. Each lane represents a single colony expressing exons $21 + 22$ or exon 21/22. (**E**) Inclusion level of exons $21 + 22$ increased from 0.52% to 6.49% with the development of cardiac hypertrophy induced by pressure overload within 14 days (n = 6). (**F–H**) Expression levels of total $Ca_V1.2$ channels and $Ca_V\beta_2$ subunits in left ventricles (n = 8). (**I,J**) Ubiquitination level of cardiac $Ca_V1.2$ channels in left ventricles (n = 8). Data were shown as mean ± SEM. $^*p < 0.05$, $^\#p < 0.01$. 1-way ANOVA was performed for multiple comparisons in panel E.

	Baseline	Day 14 post-TAC
Heart rate (bpm)	421 ± 22	$479 \pm 21^*$
LVAW; d (mm)	0.74 ± 0.03	$1.15 \pm 0.04^\S$
LVAW; s (mm)	1.00 ± 0.05	$1.41 \pm 0.06^\S$
LVPW; d (mm)	0.55 ± 0.02	$0.96 \pm 0.06^\S$
LVPW; s (mm)	0.70 ± 0.04	$1.10 \pm 0.07^\S$
LVID; d (mm)	4.25 ± 0.08	4.11 ± 0.12
LVID; s (mm)	3.35 ± 0.15	3.49 ± 0.13
LVEF (%)	49.53 ± 2.90	$33.86 \pm 2.53^\#$
FS (%)	25.05 ± 1.82	$16.18 \pm 1.45^\#$
CO (ml/min)	16.68 ± 1.11	$12.08 \pm 1.04^\#$
LV mass (mg)	74.29 ± 2.52	$135.50 \pm 11.06^\S$

Table 1. Echocardiographic characteristics of mice 0 or 14 days after TAC surgery. Echocardiography of mice 0 or 14 days after TAC surgery (n = 6). LVAW, left ventricle anterior wall thickness at end diastole (d) or end systole (s); LVPW, left ventricle posterior wall thickness; LVID, left ventricle internal dimension; LVEF, left ventricle ejection fraction; FS, fraction shortening; CO, cardiac output. $^*p < 0.05$, $^\#p < 0.01$, $^\S p < 0.001$.

(Supplementary Fig. S1). Furthermore, the heart rate of those mice was significantly increased while cardiac function was depressed as indicated by the reduction in ejection fraction and fraction shortening (Table 1).

In the hypertrophied heart, we first examined the expression level of $Ca_V1.2$ channels. Consistent with Goonasekera's report[8], total protein level of α_1 subunit of $Ca_V1.2$ channels was reduced by 40% in mouse left ventricles 14 days after TAC surgery ($p < 0.05$, Fig. 2F,G). In addition, protein level of $Ca_V\beta_2$ subunit was reduced
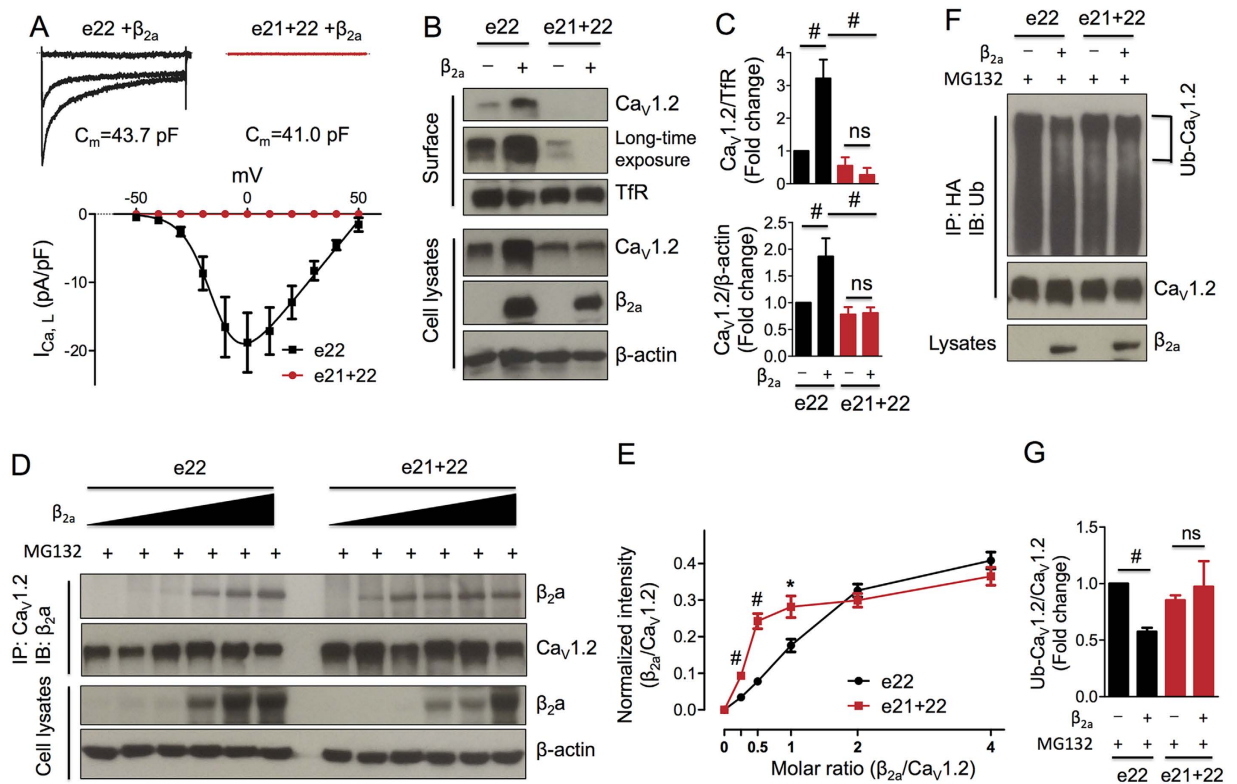
Figure 3. Characterization of exons 21 + 22-containing $Ca_V1.2_{e21+22}$ channels. (A) $Ca_V1.2_{e21+22}$ channels were co-expressed with β_{2a} and $\alpha_2\delta$ subunits in HEK293 cells. Whole cell patch-clamp recordings were performed on the cells expressing wild-type (n = 7) or **$Ca_V1.2_{e21+22}$** (n = 8) channels. **(B,C)** Detection and quantification of surface and total HA-$Ca_V1.2_{e22}$ or $Ca_V1.2_{e21+22}$ channels in the presence or absence of β_{2a} subunit in transfected HEK293 cells (n = 4). Surface channels were biotinylated as indicated in the Methods. **(D,E)** Detection and quantification of β_{2a} subunits bound to HA-$Ca_V1.2_{e22}$ or $Ca_V1.2_{e21+22}$ channels. β_{2a} subunits were co-transfected with channels at different molar ratios of 0, 1/4, 1/2, 1/1, 2/1 or 4/1 (β_{2a}/$Ca_V1.2$) in HEK293 cells treated with MG132 (2.5 μM, n = 4). **(F,G)** Detection and quantification of the ubiquitination levels of HA-$Ca_V1.2_{e22}$ and $Ca_V1.2_{-e21+22}$ channels in transfected HEK293 cells treated with MG132 (n = 3). e22, HA-$Ca_V1.2_{e22}$ channels. e21 + 22, $Ca_V1.2_{e21+22}$ channels. Data were shown as mean ± SEM, ns, non-significant, *$p < 0.05$, #$p < 0.01$.

by 45% ($p = 0.01$, Fig. 2F,H). Compared to baseline, the ubiquitination of Cav1.2 channels was clearly enhanced in the hypertrophic ventricles ($p < 0.05$, Fig. 2I,J) indicating the involvement of proteasomal degradation. Alternative splicing of Cav1.2 channels or reemergence of fetal splicing isoforms has been suggested in stressed and failing hearts[17,19], we therefore hypothesized that the neonatal isoform $Ca_V1.2_{e21+22}$ may reemerge in the adult heart in pressure overload induced hypertrophy and subsequently disturb the expression level of normal $Ca_V1.2$ channels. To test this hypothesis, transcript-screening was performed in isolated left ventricles subjected to TAC. As shown in Fig. 2D,E, the abundance of the neonatal isoform $Ca_V1.2_{e21+22}$ gradually increased by approximately 12.5-folds in the left ventricles, from 0.52% to 6.49% of total $Ca_V1.2$ channels, in 14 days of chronic pressure overload. In human hearts, the abundance of exons 21 + 22 was also significantly higher in the left ventricles from patients with dilated cardiomyopathy (DCM) than that from healthy donors (by 2.8 folds), but no elevation of exons 21 + 22 inclusion was observed in heart tissue from patients with ischemic cardiomyopathy (ICM, supplementary Fig. S2 and Table S1).

Functional characterization of $Ca_V1.2_{e21+22}$ channels. To understand the pathological significance of $Ca_V1.2_{e21+22}$ in hypertrophied heart, we characterized this isoform *in vitro* by heterologous expression in HEK 293 cells that do not have endogenous $Ca_V1.2$ channels. Compared to the robust I_{Ca} recorded from wild-type HA-tagged rat $Ca_V1.2_{e22}$ channels (-18.8 ± 3.6 pA/pF at 0 mV), no currents were detected from $Ca_V1.2_{e21+22}$ channels (Fig. 3A). Cellular localization of $Ca_V1.2_{e21+22}$ channels was examined by expression of α_1 subunit with or without β_{2a} subunit in HEK 293 cells followed by surface protein biotinylation. Consistent with a previous report[4], co-expression of β_{2a} subunit increased the surface expression level of wild-type HA-$Ca_V1.2_{e22}$ channels by 3.2-fold and the total expression level by 1.8-fold (Fig. 3B,C). However, $Ca_V1.2_{e21+22}$ channels were nearly undetectable at the cell surface regardless of the expression of β_{2a} subunit. Instead, the channel proteins were retained intracellularly (Fig. 3B,C). Of note, the total protein level of $Ca_V1.2_{e21+22}$ channels was much lower than that of wild-type channels, indicating that intracellular degradation may have occurred. Together, these data suggest that β_{2a} subunit failed to facilitate trafficking of $Ca_V1.2_{e21+22}$ channels to the cell surface.
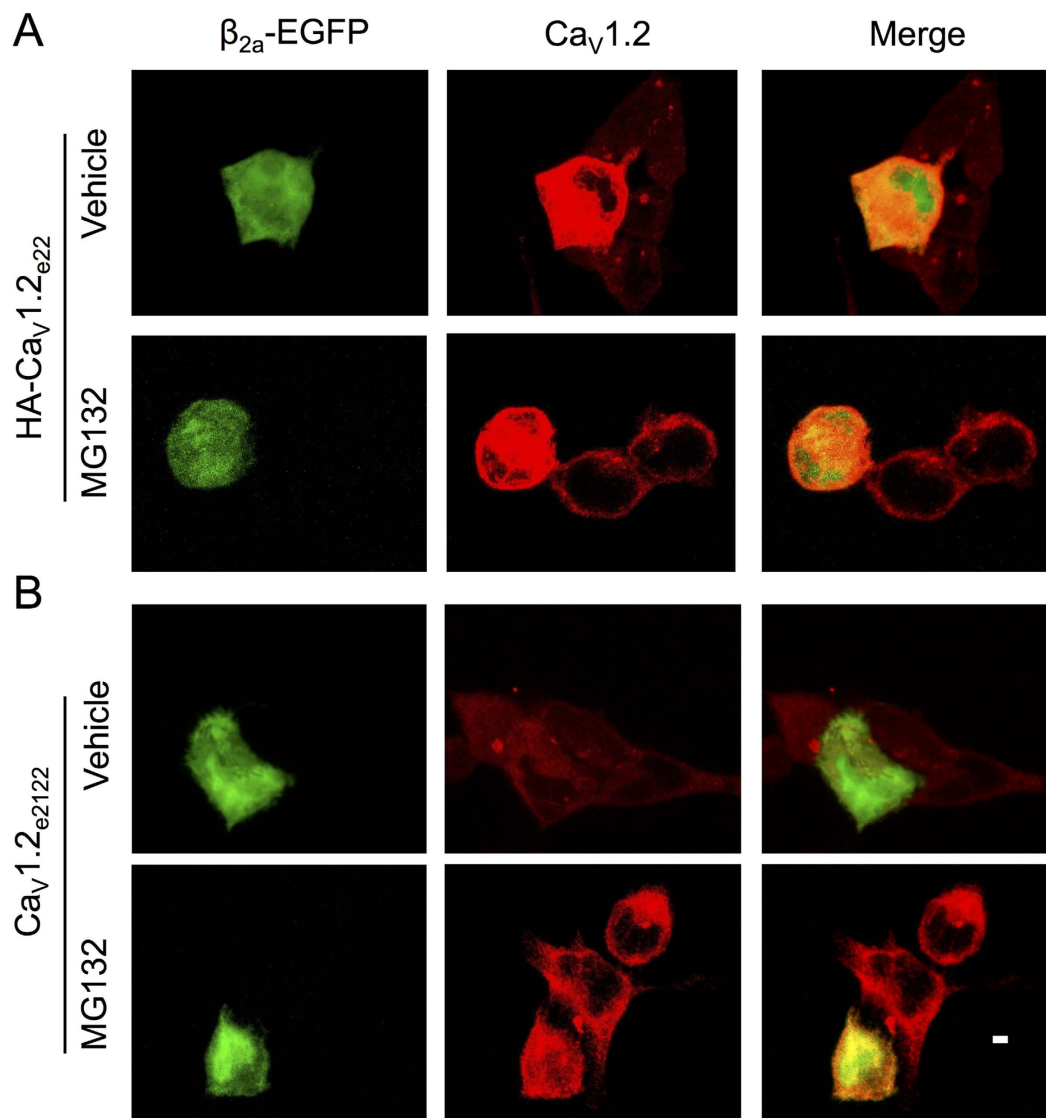
Figure 4. Ca$_V\beta$ subunits do not enhance the total expression of Ca$_V$1.2$_{e21+22}$ channels. HA-Ca$_V$1.2$_{e22}$ or Ca$_V$1.2$_{e21+22}$ were co-transfected with $\alpha_2\delta$ and β_{2a} subunit in HEK293 cells with or without MG132 treatment. β_{2a} subunit was cloned in pIRES2-EGFP (as an indicator of β_{2a} subunit expression). Immunostaining of total Ca$_V$1.2 channels and confocal imaging were performed after 48 h transfection. (**A**) β_{2a} subunit-expressing cells showed up-regulation of total HA-Ca$_V$1.2$_{e22}$ channels with or without MG132 treatment, compared to cells not expressing β_{2a} subunits. (**B**) Total Ca$_V$1.2$_{e21+22}$ channels were not markedly altered in β_{2a} subunit-expressing cells with or without MG132 treatment. Scale bar, 20 μm.

To examine whether the intracellular retention of Ca$_V$1.2$_{e21+22}$ channels was caused by attenuated binding to β_{2a} subunit, Ca$_V$1.2$_{e21+22}$ channels were co-transfected with β_{2a} subunit at different molar ratios of 0, 1/4, 1/2, 1/1, 2/1 or 4/1 (β_{2a}/Ca$_V$1.2) in HEK 293 cells in the presence of a proteasomal inhibitor, MG132 (2.5 μM). In contrast to our initial hypothesis, more β_{2a} subunits were co-immunoprecipitated by Ca$_V$1.2$_{e21+22}$ than the wild-type HA-Ca$_V$1.2$_{e22}$ channels at the molar ratios of 1/4 ($p = 0.0002$), 1/2 ($p = 0.009$), and 1/1 ($p = 0.048$) (Fig. 3D,E). Furthermore, the ubiquitination level of Ca$_V$1.2$_{e21+22}$ channels did not show significant difference in the presence or absence of β_{2a} subunit ($p = 0.65$). This is in contrast to ubiquitination of wild-type channels which was drastically reduced upon co-expression with β_{2a} subunit ($p = 0.007$, Fig. 3F,G). Taken together, the non-functional Ca$_V$1.2$_{e21+22}$ channels showed stronger interactions with β_{2a} subunit and its vulnerability to ubiquitination is not ameliorated by β_{2a} subunit.

Ca$_V\beta$ subunits did not enhance total expression of Ca$_V$1.2$_{e21+22}$ channels.

To further confirm the roles of Ca$_V\beta$ subunits in regulation of Ca$_V$1.2$_{e21+22}$ channel function, confocal microscopy was performed to image and evaluate the total expression of Ca$_V$1.2$_{e21+22}$ channels with or without β_{2a} subunits. As previously reported[4], compared to cells that did not express β_{2a} subunits, β_{2a} subunit-expressing cells showed increased expression level of total HA-Ca$_V$1.2$_{e22}$ channels with or without MG132 treatment (Fig. 4A), which is consistent
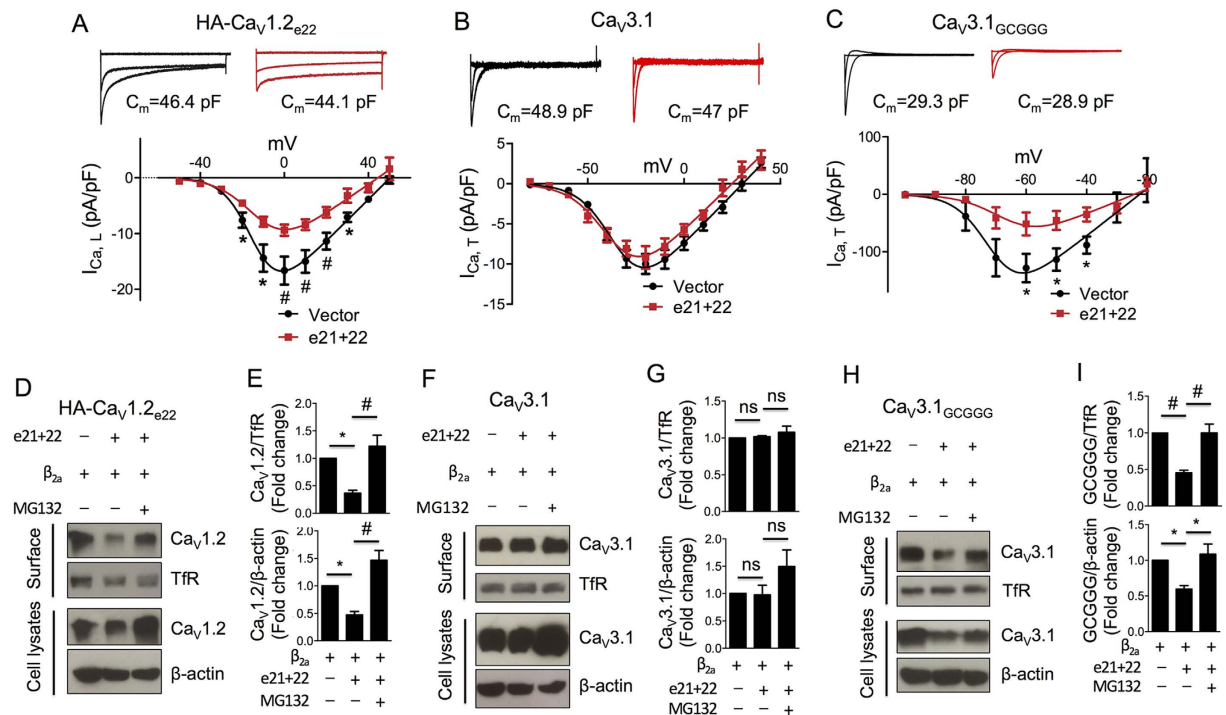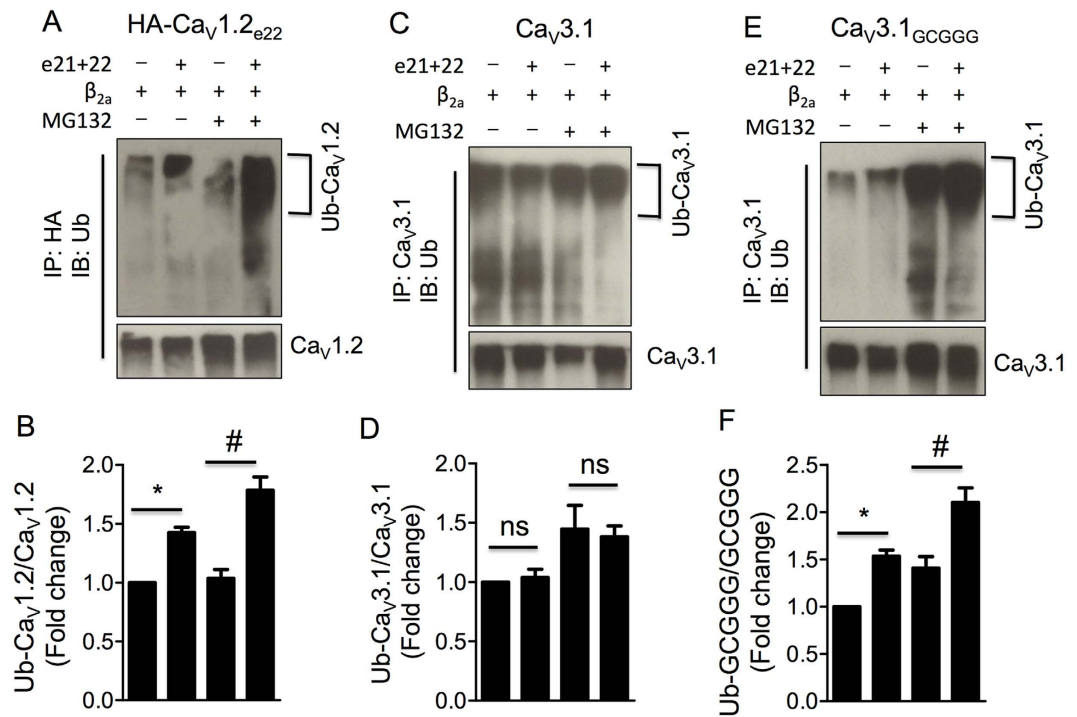
Figure 5. $Ca_V1.2_{e21+22}$ channels produce dominant-negative effects on L-type $Ca_V1.2$ channels, but not on T-type $Ca_V3.1$ channels. $Ca_V1.2_{e21+22}$ channels were co-transfected at a ratio of 1:1 with HA-$Ca_V1.2_{e22}$, $Ca_V3.1$ or chimeric $Ca_V3.1_{GCGGG}$ channels containing $Ca_V1.2$ I-II loop in HEK293 cells with or without MG132 treatment. As control, $Ca_V1.2_{e21+22}$ channels were replaced with pcDNA3 vectors for co-transfection. I-V curves were obtained in an external solution containing 1.8 mM Ca^{2+}. For western blot assays, cells were biotinylated for surface proteins 36 hrs after transfection and then lysed for analysis. (**A–C**) Effects of $Ca_V1.2_{e21+22}$ channels on the current density of wild-type $Ca_V1.2_{e22}$ channels (Vector, n = 19; e21 + 22, n = 18), $Ca_V3.1$ channels (Vector, n = 9; e21 + 22, n = 11) or the chimeric $Ca_V3.1_{-GCGGG}$ channels (Vector, n = 10; e21 + 22, n = 9). *$p < 0.05$, #$p < 0.01$. (**D–I**) Effects of $Ca_V1.2_{e21+22}$ channels on the surface and total expression levels of HA-$Ca_V1.2_{e22}$ channels (**D,E**), $Ca_V3.1$ channels (**F,G**) or chimeric $Ca_V3.1_{GCGGG}$ channels (**H,I**, n = 3). Transferrin receptor (TfR) was used as surface protein loading control. e22, wild-type HA-$Ca_V1.2_{e22}$ channel. e21 + 22, aberrant $Ca_V1.2_{e21+22}$ channel. Data were shown as mean ± SEM, ns, non-significant, *$p < 0.05$, #$p < 0.01$, 1-way ANOVA with post hoc Bonferroni's test was performed for multiple comparisons.

with the finding that ubiquitination of HA-$Ca_V1.2_{e22}$ channels was significantly reduced in the presence of β_{2a} subunits under MG132 treatment (Fig. 3F,G). However, in line with the results as shown in Fig. 3B,C, the total expression of $Ca_V1.2_{e21+22}$ channels was not markedly increased in β_{2a} subunit-expressing cells with or without MG132 treatment (Fig. 4B), which also further supported that β_{2a} subunits did not significantly prevent the ubiquitination of $Ca_V1.2_{e21+22}$ channels (Fig. 3F,G).

$Ca_V1.2_{e21+22}$ channels down-regulated expression of $Ca_V1.2_{e22}$ channels in a dominant-negative manner.
Based on the observed stronger interaction between $Ca_V1.2_{e21+22}$ channels and β_{2a} subunit, we hypothesized that $Ca_V1.2_{e21+22}$ channels may modulate the function of wild-type $Ca_V1.2$ channels by depleting or competing for free β_{2a} subunits. To test this hypothesis, $Ca_V1.2_{e21+22}$ channels were co-transfected with $Ca_V\beta$-dependent HA-$Ca_V1.2_{e22}$ channels or $Ca_V\beta$-independent $Ca_V3.1$ channels in HEK 293 cells. As measured in external solution containing 1.8 mM Ca^{2+}, the current density of $Ca_V1.2$ channels at 0 mV was lowered from -16.7 ± 2.5 pA/pF to -9.3 ± 1.0 pA/pF ($p = 0.007$, Fig. 5A). In contrast, the current density of $Ca_V3.1$ channels at -20 mV remained unchanged (-9.9 ± 1.2 pA/pF vs. -9.2 ± 1.4 pA/pF, $p = 0.671$, Fig. 5B). To further investigate whether this dominant-negative effect on $Ca_V1.2$ channels is due to reduction of free $Ca_V\beta$ subunits by $Ca_V1.2_{e21+22}$ channels, the $Ca_V1.2$ I-II loop containing the AID domain that binds $Ca_V\beta$ subunit was substituted into $Ca_V\beta$-independent $Ca_V3.1$ channel to generate a chimeric $Ca_V3.1_{GCGGG}$ channel. Compared to $Ca_V3.1$ channels, the chimeric channels displayed a dramatic increase in current amplitude and a 40 mV leftward shift in the I–V relationship (Fig. 5B,C) as previously reported[21]. Upon co-expression with $Ca_V1.2_{e21+22}$ channels, the current density of $Ca_V3.1_{GCGGG}$ channels at -60 mV was significantly reduced from -128.4 ± 22.2 pA/pF to -51.6 ± 16.8 pA/pF (Fig. 5C).

To further delineate the mechanisms underlying the differential regulation of current density by $Ca_V1.2_{e21+22}$ channels, the total and surface expression levels of all the three calcium channels were examined in HEK 293 cells co-transfected with β_{2a} subunit. As expected, $Ca_V1.2_{e21+22}$ channels did not affect the surface and total expression levels of $Ca_V3.1$ channels (Fig. 5F,G). However, co-expression of $Ca_V1.2_{e21+22}$ channels significantly reduced the surface (upper panel, Fig. 5D,E) and total (lower panel, Fig. 5D,E) levels of $Ca_V1.2$ channels and the chimeric

Figure 6. Ca$_V$1.2$_{e21+22}$ channels enhance ubiquitination of L-type Ca$_V$1.2 channels, but not T-type Ca$_V$3.1 channels. Ca$_V$1.2$_{e21+22}$ channels were co-transfected at a ratio of 1:1 with HA-Ca$_V$1.2$_{e22}$, Ca$_V$3.1 or the chimeric Ca$_V$3.1$_{GCGGG}$ channels in HEK293 cells with or without MG132 treatment. Anti-HA and anti-Ca$_V$3.1 were used to pull down the protein complexes from cell lysates for ubiquitnation analysis of HA-Ca$_V$1.2$_{e22}$ (**A,B**), wild-type Ca$_V$3.1 channels (**C,D**) or chimeric Ca$_V$3.1$_{GCGGG}$ channels (**E,F**) with or without MG132 treatment (n = 3). e22, HA-Ca$_V$1.2$_{e22}$ channel. e21 + 22, Ca$_V$1.2$_{e21+22}$ channel. Ub-Ca$_V$1.2, ubiquitinated Ca$_V$1.2 channels. Data were shown as mean ± SEM, ns, non-significant, *$p < 0.05$, #$p < 0.01$, 1-way ANOVA with post hoc Bonferroni's test was performed for multiple comparisons.

Ca$_V$3.1$_{GCGGG}$ channels (Fig. 5H,I). The reduction in expression levels of Ca$_V$β-dependent channels was prevented by MG132 treatment indicating proteasomal degradation of those channels co-expressed with the Ca$_V$1.2$_{e21+22}$ isoform (Fig. 5D,E).

Ca$_V$1.2$_{e21+22}$ channels enhanced ubiquitination of Ca$_V$β-binding calcium channels. As most proteasomal degradation involves ubiquitin, the ubiquitination levels of all the three calcium channels were evaluated in HEK 293 cells co-transfected with Ca$_V$1.2$_{e21+22}$ channels. As shown by western blot analyses, the relative intensity of ubiquitinated Ca$_V$1.2 channels (Ub-Ca$_V$1.2) to total Ca$_V$1.2 channels was greatly enhanced by the presence of Ca$_V$1.2$_{e21+22}$ channels ($p = 0.015$, Fig. 6A,B), and the increase in ubiquitination of Ca$_V$1.2 channels was augmented by MG132 treatment ($p = 0.007$, Fig. 6A,B). In contrast, the ubiquitination of Ca$_V$3.1 channels was not affected by the presence of Ca$_V$1.2$_{e21+22}$ channels or MG132 treatment (Fig. 6C,D). While introduction of the Ca$_V$β-binding domain into this Ca$_V$β-independent channel markedly increased its ubiquitination by Ca$_V$1.2$_{e21+22}$ channels (Fig. 6E,F). These results suggested that the augmentation of ubiquitination of calcium channels by Ca$_V$1.2$_{e21+22}$ channels is attributed to the Ca$_V$β-binding domain.

Ca$_V$1.2$_{e21+22}$ channels competed for Ca$_V$β subunits with Ca$_V$1.2 channels. To substantiate the notion that the reduced expression level and increased ubiquitination of Ca$_V$1.2 channels by Ca$_V$1.2$_{e21+22}$ channels were due to competition with Ca$_V$1.2 channels for available Ca$_V$β subunits, Ca$_V$1.2$_{e21+22}$ channels were co-transfected with Ca$_V$1.2, Ca$_V$3.1 or the chimeric Ca$_V$3.1$_{GCGGG}$ channels at a molar ratio of 0, 1/4, 1/2 or 1 in HEK 293 cells treated with MG132. As indicated by Western blot, the relative intensity of β$_{2a}$ subunit to Ca$_V$1.2 channels was gradually reduced with increase of Ca$_V$1.2$_{e21+22}$ channels (Fig. 7A,B). While no β$_{2a}$ subunit was co-immunoprecipitated with wild-type Ca$_V$3.1 channels (Fig. 7C) the relative intensity of β$_{2a}$ subunit to chimeric Ca$_V$3.1$_{GCGGG}$ channels was clearly attenuated by Ca$_V$1.2$_{e21+22}$ channels in a dose-dependent manner (Fig. 7D,E).

Discussion

This study identified a novel alternatively spliced isoform of Ca$_V$1.2 channels, Ca$_V$1.2$_{e21+22}$. The expression of Ca$_V$1.2$_{e21+22}$ diminishes during postnatal cardiac maturation and re-emerges in pressure-overload induced cardiac hypertrophy. This fetal-like alternative splicing pattern of Ca$_V$1.2 channels in the hypertrophied heart is in agreement with a recent report that alternative splicing events in response to TAC displayed reciprocal expression changes during postnatal cardiac development versus heart failure[22]. Despite its physiological significance during cardiac maturation, the role of the re-emergence of Ca$_V$1.2$_{e21+22}$ in response to cardiac stress is unknown.
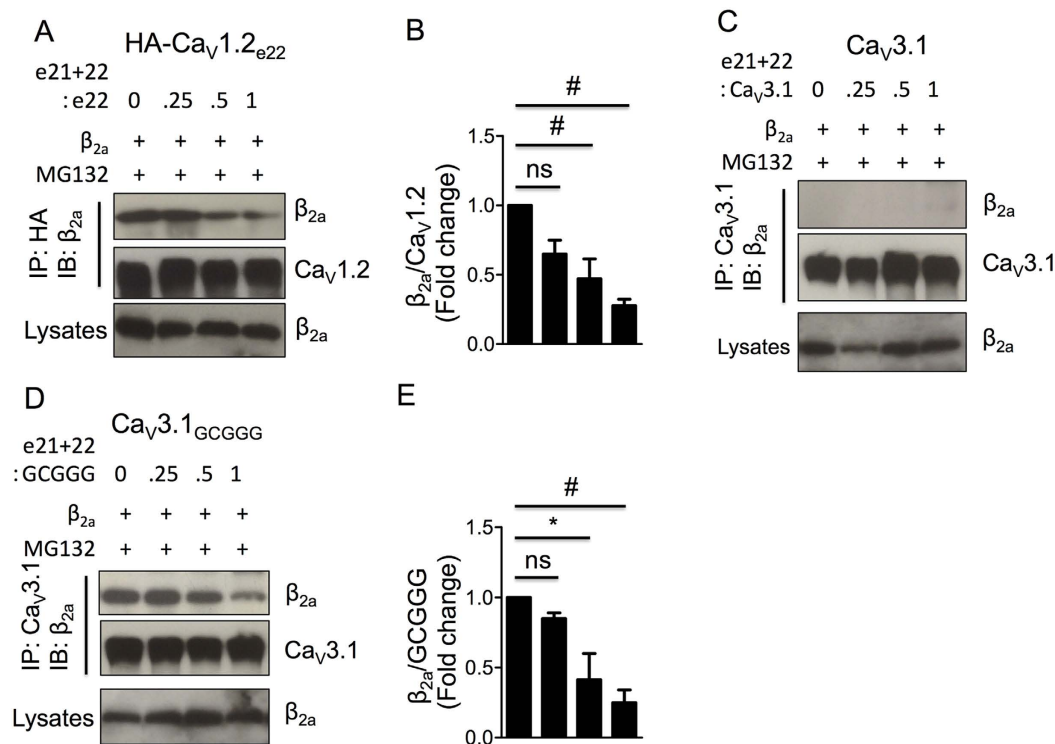
Figure 7. $Ca_V1.2_{e21+22}$ channels compete for β_{2a} subunit with L-type $Ca_V1.2$ channels, but not with T-type $Ca_V3.1$ channels, in a dose-dependent manner. $Ca_V1.2_{e21+22}$ channels were co-transfected at indicated ratios with HA-$Ca_V1.2_{e22}$, $Ca_V3.1$ or chimeric $Ca_V3.1_{GCGGG}$ channels in HEK 293 cells treated with MG132. Anti-HA and anti-$Ca_V3.1$ were used for co-immunoprecipitation. Effects of $Ca_V1.2_{e21+22}$ channels on the binding of β_{2a} subunits to HA-$Ca_V1.2_{e22}$ (**A,B**), $Ca_V3.1$ channels (**C**) or chimeric $Ca_V3.1_{GCGGG}$ channels (**E**) were analyzed by Western blotting (n = 3). e22, wild-type HA-$Ca_V1.2_{e22}$ channel. e21 + 22, aberrant $Ca_V1.2_{e21+22}$ channel. Data were shown as mean ± SEM, ns, non-significant, *$p < 0.05$, #$p < 0.01$, 1-way ANOVA with post hoc Bonferroni's test was performed for multiple comparisons.

Mutations in $Ca_V1.2$ channels are associated with multiple heart diseases including Timothy syndrome that is characterized by a long QT interval and ventricular arrhythmia due to sustained activation of $Ca_V1.2$ channels[23,24] and Brugada syndrome that is notable for a short QT interval and sudden cardiac death due to inactivation of $Ca_V1.2$ channels[25]. While the role of $Ca_V1.2$ channels in electrical heart diseases is well known, its role in mechanical or structural heart diseases remains less understood. In failing human or animal hearts, the density and currents of $Ca_V1.2$ channels were reportedly reduced[26] or unchanged[27]. In causal studies with genetic modified animals, the conclusion is so far controversial. Increase in Ca^{2+} influx through $Ca_V1.2$ channels by cardiac specific over-expression of β_{2a} subunit[7] or α_{1C} subunit[28] in mice was reported to induce cardiac hypertrophy and cardiomyopathy. Unexpectedly, decrease in Ca^{2+} influx through $Ca_V1.2$ channels in $\alpha_{1C}+/-$ mice resulted in a similar phenotype[8]. The disparities might be attributed to activation of calcineurin activation or neurohumoral effects[8]. Alternatively, it might be partly explained by the existence of two distinct subsets of the channels[24,29,30]: One subset assembled in the T-tubules for calcium-induced calcium release with ryanodine receptors for excitation-contraction coupling[31,32], and the other subset (~50% in mice)[33] enriched in caveolae to activate the transcription factor NFAT (nuclear factor of activated T cells) for cardiac hypertrophy. In line with this notion, we and Goonasekera *et al.* found that the protein level (Fig. 2) and activity of $Ca_V1.2$ channels were reduced in pressure overload-induced hypertrophic hearts[23]. Detailed analysis showed that the density and current of $Ca_V1.2$ channels both significantly declined in the isolated cardiomyocytes from those failing hearts. Although it is hard to prove which subset of channels decreased, according to their distinct functions, one may suspect that the caveolae-localized channels were affected the most in such a scenario.

One crucial question following Goonasekera's study is how the channel expression and activity was reduced in response to pressure overload. As alternative splicing occurs frequently at 19 out of 55 exons that constitute the $Ca_V1.2$ gene, *Cacna1c*, in rodent heart and artery[34,35], and some alternatively spliced isoforms were suggested to dominant-negatively suppress expression and channel conductivity of calcium channels[14,36], we therefore hypothesized that the fetal splice variant $Ca_V1.2_{e21+22}$ may reemerge in adult heart in response to cardiac stress, based on the recent findings by Gao and colleagues[22], and disrupt the expression and activity of $Ca_V1.2$ channels. In agreement with Goonasekera's findings, the total expression of $Ca_V1.2$ channels and $Ca_V\beta_2$ subunits were significantly reduced in left ventricles in response to TAC surgery (Fig. 2F–H). More importantly, the abundance of the $Ca_V1.2_{e21+22}$ splice variant in mouse left ventricles was gradually increased up to 12.5 folds within 14 days after TAC (Fig. 2), and also elevated in left ventricles of DCM patients (Supplementary Fig. S2). Aberrant splicing of

$Ca_V1.2$ channels was reported, though in very few studies, in cardiovascular diseases. For example, the abundance of exon 31- and exon 32-containing $Ca_V1.2$ isoforms significantly changed in end stage failing human hearts[17] and smooth muscle $Ca_V1.2$ channel including exon 21 was completely replaced by a single isoform containing alternative exon 22 in human atherosclerosis[18]. However, the patho-physiological significance of these splicing events is unknown.

In the present study, we demonstrated that $Ca_V1.2_{-e21+22}$ splice variant was retained intracellularly and it did not conduct Ca^{2+} (Fig. 3B,C). Strikingly, stronger binding to $Ca_V\beta$ subunit did not increase the accumulation and trafficking of $Ca_V1.2_{e21+22}$ channels to cell surface, which appears contradictory to the conceptual model proposed by the Colecraft's group[21]. In that model, it was proposed that following $Ca_V\beta$ interaction, a conformational rearrangement of the C-terminus attenuates the strength of ER retention signals within the C-terminus relative to the export signals found within the I-II loop. The net result would be enhanced trafficking to plasma membrane[21]. However, the C-terminus of rabbit $Ca_V2.1$ channels was shown to specifically interact with $Ca_V\beta_4$ subunit; meanwhile it also displayed a lower binding to $Ca_V\beta_2$ subunit[37]. In addition, Qin et $al.$ also proposed that $Ca_V\beta_{2a}$ inhibition of the inhibitory effect of $G\beta\gamma$ (G protein $\beta\gamma$ dimers) on R-type $Ca_V2.3$ channel activity could be explained by the competitive displacement of $G\beta\gamma$ from its C-terminal binding site by the $Ca_V\beta_{2a}$ subunit[38]. Based on these findings, we speculate that the presence of two transmembrane segments, exons 21 and 22, in $Ca_V1.2_{e21+22}$ channel may induce conformational changes in the C-terminus, which may lead to a stronger binding to $Ca_V\beta$ subunit and prevent the $Ca_V\beta$-dependent conformational rearrangement of the C-terminus as proposed in wild-type $Ca_V1.2$ channel. As a result, $Ca_V1.2_{e21+22}$ channels fail to be transported to cell membrane and are trapped in ER to be degraded as misfolded proteins.

$Ca_V1.2_{e21+22}$ channels suppressed expression of $Ca_V1.2$ channels via a dominant-negative mechanism. It has been shown that the misfolded calcium channels could drive wild-type channels toward proteasomal degradation, leading to a significant dominant-negative effect[14,36]. For example, the truncated variants of P/Q-type $Ca_V2.1$ channels could drive wild-type $Ca_V2.1$ channels into ER-associated degradation system by directly binding to domain I-II region[36], which required an intact N-terminus[39]. However, our data did not support a direct interaction between $Ca_V1.2_{e21+22}$ channels and wild-type $Ca_V1.2$ channels. Furthermore, the obvious dominant-negative effect of $Ca_V1.2_{-e21+22}$ channels on the chimeric $Ca_V3.1_{GCGGG}$ channels (Fig. 5) excluded a major role of the N-terminus suggested for $Ca_V2.1$ channels[39]. Therefore the dominant-negative effect of $Ca_V1.2_{e21+22}$ channels is likely attributed to a disparate mechanism. As $Ca_V1.2_{e21+22}$ channels showed significantly stronger binding to $Ca_V\beta$ subunits than that of the wild type channels, this aberrant isoform may act as a $Ca_V\beta$ subunit trap by competing for free $Ca_V\beta$ subunits. Dose-dependent inhibition of the interaction between $Ca_V\beta$ subunits and $Ca_V1.2$ or $Ca_V3.1_{GCGGG}$ channels by $Ca_V1.2_{e21+22}$ channels further supported this hypothesis. The competition for $Ca_V\beta$ subunits by $Ca_V1.2_{e21+22}$ channels may result in a shortage of free $Ca_V\beta$ subunits for $Ca_V1.2$ channels and eventually lead to impaired membrane targeting, elevated ubiquitination and thereby increased degradation of $Ca_V1.2$ channels. Accordingly, the enhanced ubiquitination and diminished expression[8] of $Ca_V1.2$ channels in the hypertrophied mouse heart induced by pressure overload are presumably caused by the reemergence of $Ca_V1.2_{e21+22}$ channels under stress (Fig. 2E). However, it is noteworthy that there are two major isoforms for $Ca_V\beta$ subunits (β_2 and β_3 subunit), quantitatively in the order of $\beta_{2b} > \beta_3 > \beta_{2a}$ in the heart[40]. Thus whether the competition for $Ca_V\beta$ subunits by $Ca_V1.2_{e21+22}$ channels is $Ca_V\beta$ isoform-dependent in cardiomyocytes will warrant further study.

Altogether, we may not anticipate that overexpression of $Ca_V1.2_{e21+22}$ channels in the heart will induce cardiac hypertrophy, rather $Ca_V1.2_{e21+22}$ channels could dominant-negatively disturb particularly the caveolae-localized $Ca_V1.2$ channels and activate the calcineurin/NFAT in response to hypertrophic stresses. Nevertheless, it is tempting to speculate that, in the patients suffering aortic stenosis or severe hypertension, $Ca_V1.2_{e21+22}$ channels may reemerge in the heart and disturb the expression and activity of $Ca_V1.2$ channels, in particular of those channels localized in the caveolae, and consequently lead to cardiac hypertrophy.

In conclusion, we have identified and functionally characterized a naturally occurring fetal splice variant of $Ca_V1.2$ channels ($Ca_V1.2_{e21+22}$ channels) that reemerged in adult mouse heart under stress and consequently disturbed the expression and activity of $Ca_V1.2$ channels. In addition, we demonstrated that this splice isoform augmented the ubiquitination of $Ca_V1.2$ channels for proteasomal degradation, impaired membrane targeting of the channels and reduced the channel expression and activity by competing for available $Ca_V\beta$ subunits. These data may provide a new insight of the dynamics of $Ca_V1.2$ channels at molecular level in the setting of cardiac hypertrophy.

Methods

Study approval.   All human heart samples obtained from Cardiovascular Research Institute, National University of Singapore (NUS), were de-identified and pre-existing. All the experiments on the human heart tissues were performed in accordance with guidelines and protocols approved by the NUS Institutional Review Board (Reference code: 12-405). One normal human heart total RNA was purchased from Clontech (636532). All animal experiments were performed in accordance with guidelines and protocols approved by the Institutional Animal Care and Use Committee of National University of Singapore.

Induction of cardiac hypertrophy in mice.   C57BL/6 mice were purchased from Jackson Laboratory and maintained at the Comparative Medicine Animal Vivarium at National University of Singapore. Experiments were carried out on adult male C57BL mice (10–12 weeks). Mice were anesthetized with a cocktail of 0.5 mg/kg Domitor, 5 mg/kg Dormicum and 0.05 mg/kg Fentanyl via intra-peritoneal injection, intubated and ventilated with a rodent ventilator (Harvard Apparatus). Transverse aortic constriction (TAC) was performed as previously described[41]. Briefly, the transverse aortic arch was exposed by a median sternotomy and bonded against a blunt 27-gauge needle with a 7-0 suture followed by prompt removal of the needle. Sham operated mice underwent the same procedure without aortic binding. Left ventricles were isolated for qPCR analysis of Myh6 and

Myh7, transcript screening of exon 21 + 22 or biochemical analysis of of $Ca_V1.2$ channels and $Ca_V\beta_2$ subunits. Echocardiography was performed with Vevo 2100 from Visualsonics.

Transcript screening. As previously described[14], total RNA was isolated using Trizol method total RNA was isolated using Trizol method from neonatal rat hearts, or left ventricles of adult rats, mice or patients with DCM or ICM. Then first strand cDNA was synthesized with Superscript II and oligo(dT)18 primers. PCR products (Primers for screening in rat heart: sense primer 5′-ACACTGCAGGTGAAGAGGATG-3′ and antisense primer 5′-TTTCCCTTGAAGAGCTGGACC-3′. For mouse heart: sense primer 5′-GAGCTGCACCTTAAGGAAAAGG-3′ and antisense primer 5′-GGATGCCAAAGGAGATGAGG-3′. For human heart: sense primer 5′-CCACCGCATTGTCAATGACAC-3′ and antisense primer 5′-CACGATGTTCCCGATGGTC-3′) were cloned into the pGEM-T Easy vector. Following transformation, each transformant was picked and grown in a single well in a 96-well plate. Colony PCR was performed with the same set of primers and conditions to identify the component of exons in each colony. 192 colonies were selected for each sample and at least 5 clones from each cDNAs group were sequenced to verify the exon specific PCR results.

DNA constructs. β_{2a} and $\alpha_2\delta$ subunits have been described previously[42]. Chimeric $Ca_V3.1_{GCGGG}$ channel[21] was kindly provided by A/Prof Henry Colecraft from Columbia University, and rat HA-$Ca_V1.2_{e22}$ channel (wild type $Ca_V1.2$ channel)[43] was from Prof Emmanuel Bourinet from Institut de Génomique Fonctionnelle. The cloning of rat $Ca_V1.2_{e21+22}$ channel was achieved by inserting a PCR fragment containing exon 21 + 22 into the wild-type channel using NotI and KpnI sites.

Cell culture and transfection. HEK293 cells were cultured in Dulbecco's Modified Eagle Medium (DMEM, Gibco) containing 10% fetal bovine serum (Gibco) and 1% penicillin–streptomycin and maintained at 37 °C in a humidified atmosphere containing 95% air and 5% CO_2. For co-immunoprecipitation experiments, if not specified, HEK293 cells were cultured in 6-well plates, and were transiently transfected with different calcium channels, β_{2a} subunit, $\alpha_2\delta$ subunit using calcium phosphate methods. In some experiments, cells were treated with a proteasomal inhibitor MG132 (2.5 μM) for 16 hrs at 24 hrs after transfection in order to prevent the proteasomal degradation of calcium channels. For whole cell patch-clamp recordings, HEK293 cells cultured on the coverslips coated with poly-D-lysine in 35 mm dishes were transiently transfected with different calcium channels at a molar ratio of 1:1 unless otherwise stated.

Co-immunoprecipitation. Co-immunoprecipitation was performed as described previously with modification. In brief, proteins harvested from transfected HEK293 cells were incubated with primary antibodies overnight at 4 °C with gentle rotation, followed by incubation with 20 μl of protein A/G agarose (Pierce) for another 1 h at 4 °C. The beads were washed 3 times using cold PBS and then denatured in 2X SDS sample loading buffer by boiling at 95 °C for 10 min. Proteins were then used for western blot analysis.

Surface protein biotinylation. To determine the level of $Ca_V1.2_{e21+22}$ channels localized on the cell surface, $Ca_V1.2_{e21+22}$ channels were biotinylated using an EZ-Link™ Sulfo-NHS-Biotinylation Kit (Pierce) as previously described with modifications[44]. Briefly, cells were incubated with 0.25 mg/ml Biotin for 1h at 4 °C. Unbound biotin was removed by incubation with quenching buffer for 20 min and washed by PBS buffer. After measurement of protein concentration with Bradford assay, cell lysates were incubated with NeutrAvidin (Pierce) overnight to pull down the biotinylated surface proteins. The precipitates were boiled in 2X sample loading buffer to elute Avidin-bound for SDS-PAGE analysis. GAPDH was used as a cytoplasmic marker to assess whether the surface biotinylated fractions include cytoplasmic channels (Data were not included).

Ubiquitination assay. $Ca_V1.2_{e21+22}$ channels were transiently transfected with HA-$Ca_V1.2_{e22}$, wild-type $Ca_V3.1$ or chimeric $Ca_V3.1_{GCGGG}$ channels in HEK 293 cells. Twenty-four hours after transfection, cells were treated with MG132 (2.5 μM) overnight and then lysed in PBS buffer containing 1% SDS and 1 mM EDTA. Cell lysates were boiled for 5 min at 95 °C, votexed for 10 sec, and then boiled for another 3 min at 95 °C. Ubiquitinated substrates in the supernatant were immunoprecipitated with anti-$Ca_V3.1$ or anti-HA, washed 3 times with cold PBS buffer, and resolved by 8% SDS-PAGE gel.

Western blot. Cells were harvested using lysis buffer (50 mM Tris, 150 mM NaCl, 1 mM EDTA, 1% Triton X-100, pH 7.4) containing protease inhibitor cocktails (Roche) at 48 hrs after transfection. After measurement of protein concentration, cell lysates were separated by 8% SDS-PAGE for 50 min at 150 V and transferred onto PVDF membrane at 30 V overnight at 4 °C. Subsequently, the membrane was blocked with 5% non-fat milk for 1h at room temperature and then incubated overnight at 4 °C with primary antibodies: rabbit anti-$Ca_V1.2$ (1:1000, ACC-003, Alomone), anti-$Ca_V3.1$ (1:1000, ACC-021), rabbit anti-β_2 (1:1000, ACC-105), mouse anti-ubiquitin (1:1000, 13–1600, Invitrogen), rabbit anti-HA (1:1000, 71–5500), mouse anti-TfR (1:1000, 13–6800), mouse anti-β-actin (1:5000, A1978, Sigma) or mouse anti-GAPDH (1:2000, G8795). The membrane was washed three times with TBS-T buffer and then incubated with corresponding HRP-conjugated secondary antibodies (1:5000) for 1h at room temperature. After washing, proteins were detected using West Pico or Femto Chemiluminescent Substrate (Pierce). The blots were analyzed with ImageJ software (NIH).

Confocal imaging. HA-$Ca_V1.2_{e22}$ or $Ca_V1.2_{e21+22}$, $\alpha_2\delta$ and β_{2a} subunit in pIRES2-EGFP as an indicator of β_{2a} subunit expression were co-transfected in HEK293 cells cultured in 35 mm dish using calcium phosphate method. As described previously[4], 48 h after transfection, cells were passaged to 2 wells with coated coverslips in 12-well plate, followed by 10 μM MG132 treatment for 2 h with cells in one of the wells. After that, cells were washed by cold PBS containing 5% FBS and fixed in 4% paraformaldehyde for 15 min. Following permeablization

using 0.2% Tween-20/PBS for 15 min and blocking by 10% FBS/PBS for 20 min, cells were stained with rabbit anti-$Ca_V1.2$ (1:100, Alomone) at 37 °C for 60 min. Alexa Fluor 594-conjugated goat α-rabbit IgG antibody (Molecular Probes, 1:300) was used as secondary antibody to incubate with cells for 60 min in room temperature.

Cells were imaged using a Zeiss LSM-510 Meta confocal microscope with a 63 × 1.4NA oil immersion lens in the inverted position. EGFP was visualized by excitation with an argon laser (488 nm) and emission detected using a long-pass 530-nm filter. AF-594 antibody was visualized by excitation with a HeNe laser (543 nm) and emission detected using a 585–615 nm bandpass filter. Image acquisition was performed with identical gain, contrast, laser excitation, pinhole aperture and laser scanning speed for 3 rounds of cultures.

Electrophysiological recordings. As previously described, patch-clamp recordings were performed at 24–72 hrs after transfection using an Axopatch 200B amplifier (Molecular Device). The external solution contained 144 mM TEA-MeSO$_3$, 10 mM HEPES, 1.8 mM CaCl$_2$ (pH 7.4 adjusted with CsOH and osmolarity 300–310 mOsm with glucose). The internal solution contained 138 mM Cs-MeSO$_3$, 5 mM CsCl, 0.5 mM EGTA, 10 mM HEPES, 1 mM MgCl$_2$, 2 mg/ml Mg-ATP (pH 7.3 adjusted with CsOH and osmolarity 300–310 mOsm with glucose). To determine the whole cell current-voltage (*I-V*) relationships, currents were recorded by holding the cell at −90 mV (or −100 mV for $Ca_V3.1_{GCGGG}$ channel) before stepping to various potentials from −90 to 60 mV (or −100 to 40 mV for $Ca_V3.1_{GCGGG}$ channel) over 900 ms. The *I-V* curve was fitted with the equation: $I_{Ca} = G_{max}(V - E_{rev})/(1 + \exp((V - V_{1/2})/k))$, where G_{max} is the maximum conductance; E_{rev} is the reversal potential; $V_{1/2}$ is the half-activation potential; and k is the slope.

Statistics. All results were presented as mean ± SEM. Student's *t* test was performed to compare two independent groups and one-way ANOVA followed by Bonferroni post hoc test was used for multiple group comparisons. $P < 0.05$ was considered significant.

References

1. Hofmann, F., Flockerzi, V., Kahl, S. & Wegener, J. W. L-type $Ca_V1.2$ calcium channels: from *in vitro* findings to *in vivo* function. *Physiol Rev* **94**, 303–326, doi: 10.1152/physrev.00016.2013 (2014).
2. Dolphin, A. C. Calcium channel auxiliary alpha2delta and beta subunits: trafficking and one step beyond. *Nat Rev Neurosci* **13**, 542–555, doi: 10.1038/nrn3311(2012).
3. Catterall, W. A. Voltage-gated calcium channels. *Cold Spring Harb Perspect Biol* **3**, a003947, doi: 10.1101/cshperspect.a003947 (2011).
4. Altier, C. *et al.* The Cavbeta subunit prevents RFP2-mediated ubiquitination and proteasomal degradation of L-type channels. *Nat Neurosci* **14**, 173–180, doi: 10.1038/nn.2712 (2011).
5. Weissgerber, P. *et al.* Reduced cardiac L-type Ca2+ current in Ca(V)beta2-/- embryos impairs cardiac development and contraction with secondary defects in vascular maturation. *Circ Res* **99**, 749–757, doi: 10.1161/01.RES.0000243978.15182.c1 (2006).
6. Seisenberger, C. *et al.* Functional embryonic cardiomyocytes after disruption of the L-type alpha1C (Cav1.2) calcium channel gene in the mouse. *J Biol Chem* **275**, 39193–39199, doi: 10.1074/jbc.M006467200 (2000).
7. Chen, X. *et al.* Calcium influx through Cav1.2 is a proximal signal for pathological cardiomyocyte hypertrophy. *J Mol Cell Cardiol* **50**, 460–470, doi: 10.1016/j.yjmcc.2010.11.012 (2011).
8. Goonasekera, S. A. *et al.* Decreased cardiac L-type Ca(2)(+) channel activity induces hypertrophy and heart failure in mice. *J Clin Invest* **122**, 280–290, doi: 10.1172/JCI58227 (2012).
9. Patel, K. *et al.* Calcium channel blockers and outcomes in older patients with heart failure and preserved ejection fraction. *Circ Heart Fail* **7**, 945–952, doi: 10.1161/CIRCHEARTFAILURE.114.001301 (2014).
10. de Vries, R. J., van Veldhuisen, D. J. & Dunselman, P. H. Efficacy and safety of calcium channel blockers in heart failure: focus on recent trials with second-generation dihydropyridines. *Am Heart J* **139**, 185–194 (2000).
11. Packer, M. *et al.* Effect of amlodipine on the survival of patients with severe chronic heart failure due to a nonischemic cardiomyopathy: results of the PRAISE-2 study (prospective randomized amlodipine survival evaluation 2). *JACC Heart Fail* **1**, 308–314, doi: 10.1016/j.jchf.2013.04.004 (2013).
12. Chen, X. *et al.* L-type Ca2+ channel density and regulation are altered in failing human ventricular myocytes and recover after support with mechanical assist devices. *Circ Res* **91**, 517–524 (2002).
13. Tang, Z. Z. *et al.* Transcript scanning reveals novel and extensive splice variations in human l-type voltage-gated calcium channel, Cav1.2 alpha1 subunit. *J Biol Chem* **279**, 44335–44343, doi: 10.1074/jbc.M407023200 (2004).
14. Liao, P. *et al.* Alternative splicing generates a novel truncated Cav1.2 channel in neonatal rat heart. *J Biol Chem* **290**, 9262–9272, doi: 10.1074/jbc.M114.594911 (2015).
15. Tang, Z. Z., Zheng, S., Nikolic, J. & Black, D. L. Developmental control of CaV1.2 L-type calcium channel splicing by Fox proteins. *Mol Cell Biol* **29**, 4757–4765, doi: 10.1128/MCB.00608-09 (2009).
16. Liao, P. *et al.* Molecular alteration of Ca(v)1.2 calcium channel in chronic myocardial infarction. *Pflugers Arch* **458**, 701–711, doi: 10.1007/s00424-009-0652-4 (2009).
17. Yang, Y. *et al.* L-type Ca2+ channel alpha 1c subunit isoform switching in failing human ventricular myocardium. *J Mol Cell Cardiol* **32**, 973–984, doi: 10.1006/jmcc.2000.1138 (2000).
18. Tiwari, S., Zhang, Y., Heller, J., Abernethy, D. R. & Soldatov, N. M. Atherosclerosis-related molecular alteration of the human CaV1.2 calcium channel alpha1C subunit. *Proc Natl Acad Sci USA* **103**, 17024–17029, doi: 10.1073/pnas.0606539103 (2006).
19. Gidh-Jain, M., Huang, B., Jain, P., Battula, V. & el-Sherif, N. Reemergence of the fetal pattern of L-type calcium channel gene expression in non infarcted myocardium during left ventricular remodeling. *Biochem Biophys Res Commun* **216**, 892–897 (1995).
20. Sano, M. *et al.* p53-induced inhibition of Hif-1 causes cardiac dysfunction during pressure overload. *Nature* **446**, 444–448, doi: 10.1038/nature05602 (2007).
21. Fang, K. & Colecraft, H. M. Mechanism of auxiliary beta-subunit-mediated membrane targeting of L-type (Ca(V)1.2) channels. *J Physiol* **589**, 4437–4455, doi: 10.1113/jphysiol.2011.214247 (2011).
22. Gao, C. *et al.* RBFox1-mediated RNA splicing regulates cardiac hypertrophy and heart failure. *J Clin Invest* **126**, 195–206, doi: 10.1172/JCI84015 (2016).
23. Splawski, I. *et al.* Ca(V)1.2 calcium channel dysfunction causes a multisystem disorder including arrhythmia and autism. *Cell* **119**, 19–31, doi: 10.1016/j.cell.2004.09.011 (2004).
24. Dixon, R. E., Cheng, E. P., Mercado, J. L. & Santana, L. F. L-type Ca2+ channel function during Timothy syndrome. *Trends Cardiovasc Med* **22**, 72–76, doi: 10.1016/j.tcm.2012.06.015 (2012).
25. Antzelevitch, C. *et al.* Loss-of-function mutations in the cardiac calcium channel underlie a new clinical entity characterized by ST-segment elevation, short QT intervals, and sudden cardiac death. *Circulation* **115**, 442–449, doi: 10.1161/CIRCULATIONAHA.106.668392 (2007).

26. Ming, Z., Nordin, C., Siri, F. & Aronson, R. S. Reduced calcium current density in single myocytes isolated from hypertrophied failing guinea pig hearts. *J Mol Cell Cardiol* **26,** 1133–1143, doi: 10.1006/jmcc.1994.113 (1994).

27. Mewes, T. & Ravens, U. L-type calcium currents of human myocytes from ventricle of non-failing and failing hearts and from atrium. *J Mol Cell Cardiol* **26,** 1307–1320, doi: 10.1006/jmcc.1994.1149 (1994).

28. Wang, S. *et al.* Dilated cardiomyopathy with increased SR Ca2+ loading preceded by a hypercontractile state and diastolic failure in the alpha(1C)TG mouse. *PLoS One* **4,** e4133, doi: 10.1371/journal.pone.0004133 (2009).

29. Glukhov, A. V. *et al.* Direct Evidence for Microdomain-Specific Localization and Remodeling of Functional L-Type Calcium Channels in Rat and Human Atrial Myocytes. *Circulation* **132,** 2372–2384, doi: 10.1161/CIRCULATIONAHA.115.018131 (2015).

30. Makarewich, C. A. *et al.* A caveolae-targeted L-type Ca(2)+ channel antagonist inhibits hypertrophic signaling without reducing cardiac contractility. *Circ Res* **110,** 669–674, doi: 10.1161/CIRCRESAHA.111.264028 (2012).

31. Horiuchi-Hirose, M. *et al.* Decrease in the density of t-tubular L-type Ca2+ channel currents in failing ventricular myocytes. *Am J Physiol Heart Circ Physiol* **300,** H978–H988, doi: 10.1152/ajpheart.00508.2010 (2011).

32. Kashihara, T. *et al.* beta(2)-Adrenergic and M(2)-muscarinic receptors decrease basal t-tubular L-type Ca2+ channel activity and suppress ventricular contractility in heart failure. *Eur J Pharmacol* **724,** 122–131, doi: 10.1016/j.ejphar.2013.12.037 (2014).

33. Nichols, C. B. *et al.* Sympathetic stimulation of adult cardiomyocytes requires association of AKAP5 with a subpopulation of L-type calcium channels. *Circ Res* **107,** 747–756, doi: 10.1161/CIRCRESAHA.109.216127 (2010).

34. Liao, P., Zhang, H. Y. & Soong, T. W. Alternative splicing of voltage-gated calcium channels: from molecular biology to disease. *Pflugers Arch* **458,** 481–487, doi: 10.1007/s00424-009-0635-5 (2009).

35. Cheng, X. *et al.* Alternative splicing of Cav1.2 channel exons in smooth muscle cells of resistance-size arteries generates currents with unique electrophysiological properties. *Am J Physiol Heart Circ Physiol* **297,** H680–H688, doi: 10.1152/ajpheart.00109.2009 (2009).

36. Mezghrani, A. *et al.* A destructive interaction mechanism accounts for dominant-negative effects of misfolded mutants of voltage-gated calcium channels. *J Neurosci* **28,** 4501–4511, doi: 10.1523/JNEUROSCI.2844-07.2008 (2008).

37. Walker, D., Bichet, D., Campbell, K. P. & De Waard, M. A beta 4 isoform-specific interaction site in the carboxyl-terminal region of the voltage-dependent Ca2+ channel alpha 1A subunit. *J Biol Chem* **273,** 2361–2367 (1998).

38. Qin, N., Platano, D., Olcese, R., Stefani, E. & Birnbaumer, L. Direct interaction of gbetagamma with a C-terminal gbetagamma-binding domain of the Ca2+ channel alpha1 subunit is responsible for channel inhibition by G protein-coupled receptors. *Proc Natl Acad Sci USA* **94,** 8866–8871 (1997).

39. Page, K. M. *et al.* N terminus is key to the dominant negative suppression of Ca(V)2 calcium channels: implications for episodic ataxia type 2. *J Biol Chem* **285,** 835–844, doi: 10.1074/jbc.M109.065045 (2010).

40. Hullin, R. *et al.* Cardiac L-type calcium channel beta-subunits expressed in human heart have differential effects on single channel characteristics. *J Biol Chem* **278,** 21623–21630, doi: 10.1074/jbc.M211164200 (2003).

41. Rockman, H. A. *et al.* Segregation of atrial-specific and inducible expression of an atrial natriuretic factor transgene in an *in vivo* murine model of cardiac hypertrophy. *Proc Natl Acad Sci USA* **88,** 8277–8281 (1991).

42. Wang, J. *et al.* Splice variant specific modulation of CaV1.2 calcium channel by galectin-1 regulates arterial constriction. *Circ Res* **109,** 1250–1258, doi: 10.1161/CIRCRESAHA.111.248849 (2011).

43. Altier, C. *et al.* Trafficking of L-type calcium channels mediated by the postsynaptic scaffolding protein AKAP79. *J Biol Chem* **277,** 33598–33603, doi: 10.1074/jbc.M202476200 (2002).

44. Bannister, J. P. *et al.* Ca(V)1.2 channel N-terminal splice variants modulate functional surface expression in resistance size artery smooth muscle cells. *J Biol Chem* **286,** 15058–15066, doi: 10.1074/jbc.M110.182816 (2011).

Acknowledgements

Author Contributions

T.W.S. conceived and supervised this project. Z.H. performed most of the biochemical assays. J.-W.W. generated the TAC mouse models, evaluated the cardiac function of TAC mice and harvested the left ventricles. D.Y. and Z.H. conducted the path-clamp recordings. Z.H. and J.-W.W. wrote the initial draft of the manuscript. T.W.S., P.L., H.M.C., D.P.V.d.K., J.L.S. and R.F. edited the manuscript.

Additional Information

Supplementary information accompanies this paper at http://www.nature.com/srep

Competing financial interests: The authors declare no competing financial interests.

How to cite this article: Hu, Z. *et al.* Aberrant Splicing Promotes Proteasomal Degradation of L-type Ca$_V$1.2 Calcium Channels by Competitive Binding for Ca$_V$β Subunits in Cardiac Hypertrophy. *Sci. Rep.* **6,** 35247; doi: 10.1038/srep35247 (2016).